

Diamond turned high precision PIAA optics and four mirror PIAA system for high contrast imaging of exo-planets

Kunjithapatham Balasubramanian^{a*}, Eric Cady^a, Laurent Pueyo^{b,c}, Xin An^a, Stuart Shaklan^a, Olivier Guyon^{d,e} and Ruslan Belikov^f

^aJet Propulsion Laboratory, California Institute of Technology, Pasadena, CA 91109, USA

^bJohns Hopkins University, Baltimore, MD 21218, USA ^cSagan Fellow

^dSteward Observatory, The University of Arizona, Tucson, AZ 85721, USA

^eSubaru Telescope, National Astronomical Observatory of Japan, Hilo, HI 96720, USA

^fNASA Ames Research Center, Moffett Field, CA 94035, USA

ABSTRACT

Off-axis, high-sag PIAA optics for high contrast imaging present challenges in manufacturing and testing. With smaller form factors and consequently smaller surface deformations (< 80 microns), diamond turned fabrication of these mirrors becomes feasible. Though such a design reduces the system throughput, it still provides $2\lambda/D$ inner working angle. We report on the design, fabrication, measurements, and initial assessment of the novel PIAA optics in a coronagraph testbed. We also describe, for the first time, a four mirror PIAA coronagraph that relaxes apodizer requirements and significantly improves throughput while preserving the low-cost benefits.

1. INTRODUCTION

Phase-induced amplitude apodization (PIAA) is a concept for high-contrast imaging which uses shaped mirrors to losslessly adjust the amplitude profile of an incoming wavefront. Following the introduction of the concept of PIAA in 2003,^{1,2} research in various labs have achieved different levels of image contrast over the past few years. In 2010,³ we proposed designing, manufacturing and testing conservatively low-sag PIAA mirrors by conventional diamond-turning techniques⁴ inexpensively and efficiently. Such an approach allowed fast turn-around for testing concepts, though with a mild compromise on performance. A review of these concepts and some results from the testbed at NASA Ames are given in Section 2. These low-sag mirrors require a post-apodizer to achieve their full performance potential, which can cause throughput reduction. We have now designed a 4-mirror PIAA system, which uses a second set of mirrors to perform the job of the post-apodizer without throughput losses. A design and some preliminary investigations of the manufactured mirrors are given in Section 3.

2. TWO-MIRROR LOW-SAG PIAA SYSTEM

Constraining the mirror sag to ~ 30 microns, a two-mirror PIAA system was designed with 30mm diameter mirrors as detailed in our 2010 paper.³ Employing low-thermal-expansion super-Invar blanks plated with a layer of Ni, a pair of low-sag PIAA mirrors with a footprint of 30mm were manufactured by a diamond-turning technique. The mirrors are fabricated with a flat annulus outside the PIAA region. These are used to co-align the mirrors. To measure the wavefront error of the output beam of the PIAA pair, first a reference flat is aligned to the Zygo interferometer to fluff out the interference fringes, as shown in Fig. 1. Then M1 and M2 are inserted, partially blocking the beam. M2 is tilted until the fringes in the annular region are fluffed out. The mirrors are then parallel to one another. Then M2 is translated to find the best position. This approach decouples tip/tilt from translation. The mirrors are circularly symmetric so there is no need to rotate about the central axis. The distance between M1 and M2 is optimized by iteratively translating and

* Corresponding author: kbala@jpl.nasa.gov; phone: 818-393-0258

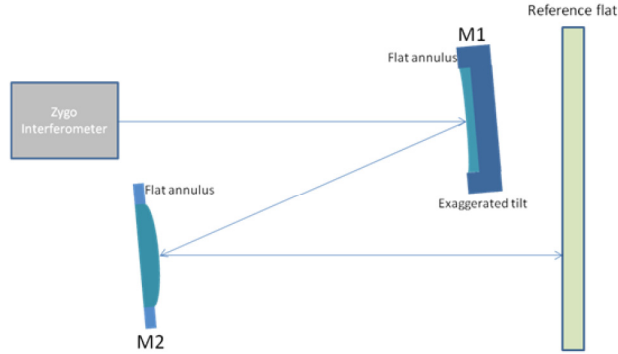


Figure 1. A Zygo interferometer set up with a PIAA pair to measure wavefront error in a double-pass configuration.

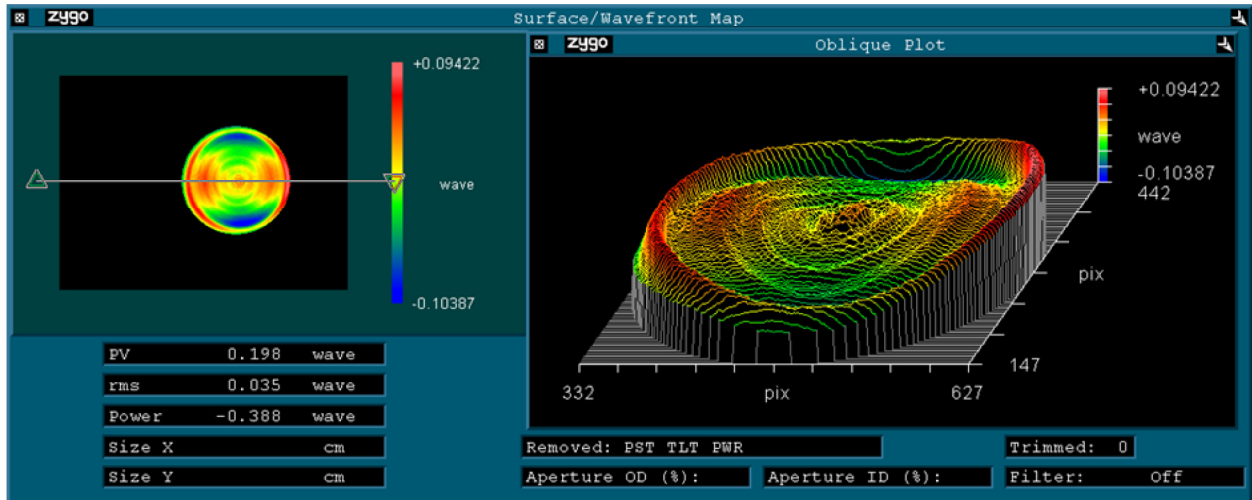


Figure 2. Wavefront error of an aligned Ni/Superinvar M1-M2 PIAA pair as measured with a Zygo interferometer in double-pass.

tilting until minimum wavefront error (WFE) is obtained with minimum residual power. The residual WFE is mainly due to astigmatism introduced by the tilt in the set up as shown in Fig. 1. The DMs employed in the coronagraph testbed can ultimately compensate for such small errors. Fig. 2 shows the wavefront error of collimated beam from this pair of mirrors as measured in double-pass. The sensitivity of the alignment with M1-M2 separation is shown in Fig. 3.

2.1 Preliminary nulling experiment and contrast measurement at NASA Ames coronagraph testbed

This Ni/Superinvar pair of PIAA mirrors with 30mm foot print and 35 micron sag were recently tested at NASA Ames Research Center (ARC) coronagraph testbed. Figure 4 shows the final image with average monochromatic contrast of 5.5×10^{-7} in the nulled region covering 3.5 to $5\lambda/D$. This result was mainly limited by instabilities in the system, which have been subsequently improved for other experiments. Some additional discussion can be found in Belikov *et al.* 2011.⁵

3. FOUR-MIRROR DESIGN

To design a four-mirror system, we start by considering the properties of a standard two-mirror PIAA radially-symmetric system. Barring the effects of diffraction, which we will return to later, a PIAA remapping

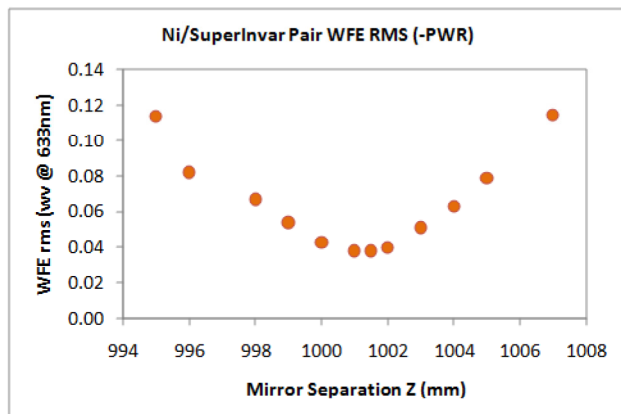


Figure 3. WFE alignment sensitivity to M1-M2 separation distance.

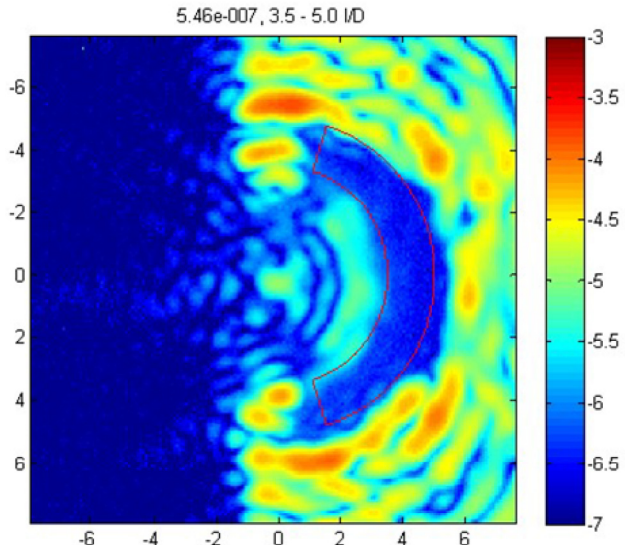


Figure 4. The dark hole in the nulled region, obtained with low-sag PIAA mirror pair.

system can be thought of as consisting of three amplitude profiles. First, we have the initial amplitude profile of the field incident on the first mirror, which we denote $A_i(r)$. When a pre-apodizer is present, it will define $A_i(r)$; otherwise, it will be a flat-top beam with radius equal to the radius of the first mirror, R . Second, we have the corresponding final amplitude at the output of the second mirror, which we denote $A_f(r)$. This will not include a post-apodizer, which can be added later. The final profile we term the “intrinsic” profile of the mirror pair, denoted $A_m(r)$, and is the amplitude profile one would expect from ray optics and an incident plane wave. Notationally, this is equivalent to $\sqrt{f_2(r)}$ in Guyon 2003¹ and $A(\tilde{r})$ in Vanderbei and Traub 2005.⁶ These three profiles are not independent; it can be shown⁷ that given any two, the third can be derived. (As a well-designed PIAA system should have uniform phase across its input and output, we will concentrate solely on amplitude for the moment.)

A four-mirror system uses two mirror pairs in series, each with its own set of amplitude profiles. (A diagram is shown in Fig. 5.) To link them together, we require that a basic matching condition be met:

$$A_{i,2}(r) = A_{f,1}(r) \quad (1)$$

with the numerical subscripts denoting the first and second pair. This method allows us the freedom to set the desired amplitude profile for the output of the four-mirror system and the preapodization, as well as the intrinsic profile of one pair of mirrors. The primary advantage to this approach is that the second pair of mirrors can be used to do the job of a post-apodizer, providing a portion of the total beam shaping without a loss of throughput, as well as providing additional magnification. In exchange, the system becomes more complex, requiring precise alignment of four mirrors to produce the correct beam. It also doubles the total cost of the system mirrors, although with diamond-turned mirrors the four mirrors can still be completed for under \$10K.

For our purposes, $A_{f,2}(r)$ and $A_{m,2}(r)$ are both chosen as Gaussians, with appropriate scaling factors to ensure full throughput:

$$A_{f,2}(r) \propto e^{-10\left(\frac{r}{R}\right)^2} \quad (2)$$

$$A_{m,2}(r) \propto e^{-2\left(\frac{r}{R}\right)^2} \quad (3)$$

Neither choice is necessarily unique for this application. $A_{f,2}(r)$ is chosen as a Gaussian based on the observations of Belikov *et al.*,⁸ who have found Gaussian amplitude profiles to provide adequate suppression

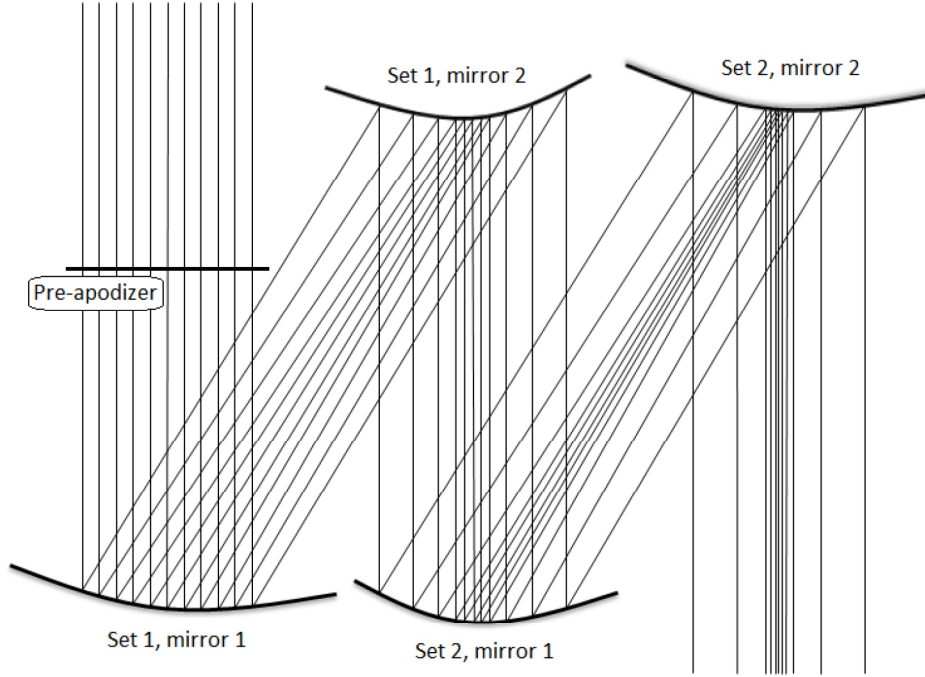


Figure 5. The positions of the four mirrors and the preapodizer in a 4-mirror system.

at small inner working angle in the image plane. The choice of $A_{m,2}(r)$ as a Gaussian is primarily driven by the observation⁷ that $A_{i,2}(r)$ can be expressed analytically for both $A_{f,2}(r)$ and $A_{m,2}(r)$ Gaussian, which simplifies the derivation of $A_{m,1}(r)$; the coefficient 2 in the exponent was found after a certain amount of iteration to produce nearly identical sag on both sets of mirrors. As a preapodizer, we use:

$$A_{i,1}(r) = \begin{cases} 1, & r \leq R_p \\ a + 3(b-a) \left(\frac{r-R_p}{R-R_p} \right)^2 + 2(a-b) \left(\frac{r-R_p}{R-R_p} \right)^3, & R_p \leq r \leq R \\ 0, & r \geq R \end{cases} \quad (4)$$

with $R_p = 0.9$, $b = 0.012$, and $a = 1$. As with $A_{m,2}(r)$, this choice is driven by certain useful numerical properties more than any optimal performance considerations. As mentioned above, $A_{m,1}(r)$ is determined exactly by $A_{i,1}(r)$ and $A_{m,2}(r)$.

For the laboratory system, Fig. 6 shows the shape of the inner 15mm radius of all four mirrors, and Fig. 7 the resulting performance: the system would provide 10^{-9} suppression beyond $1.5 \lambda/D$ on-sky.

This design was created using amplitude profiles, but subsequently modeled and adjusted using a full diffraction model based around S-Huygens propagation.^{9,10} It can be shown⁷ that the electric field resulting from full diffraction calculations can be written as a term identical to the one from geometric optics, with additional higher order terms from the stationary phase approximation perturbing this slightly. These terms depend on both the mirror radius R and the mirror spacing z , and can be mitigated somewhat by choosing large mirrors and small spacing. Additionally, we can provide an empirical correction by recalling that the main purpose of the second mirror in a PIAA set is to redirect the light to restore a uniform phase profile; we can perturb this surface based on the phase profile after the mirror pair from diffraction to improve performance. Both of these techniques were used in the design of the above four-mirror system, to provide 1.5×10^{-9} average contrast at $1.5\lambda/D$ and beyond in a 20% band around 633nm. (We note that 10^{-9} is not a fundamental limitation of a four-mirror system, but was rather limited by choices of R , z , and limitations on mirror sag, chosen conservatively.)

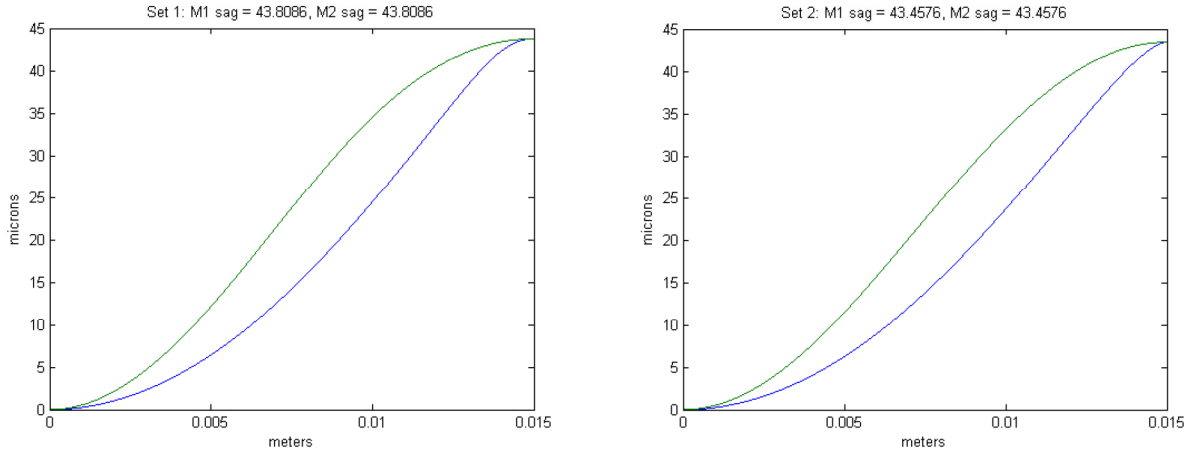


Figure 6. The shapes of the two pairs of mirrors in the four-mirror system. In each case, the first mirror in each set is blue and the second is green.

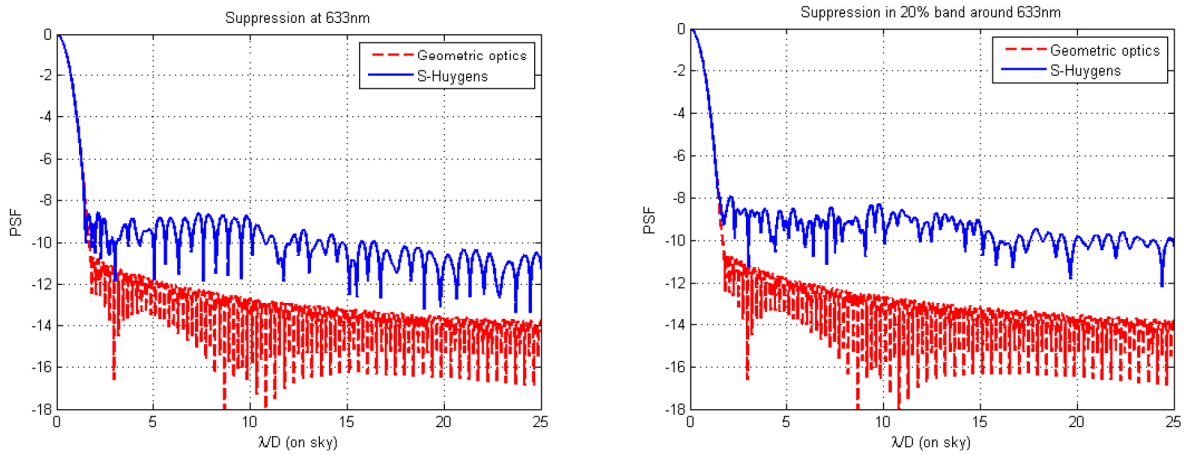


Figure 7. A comparison of the theoretical performance of the 4-mirror system based on geometric optics, and the performance with diffraction effects included. *Left.* Performance at 633nm. *Right.* Performance in a 20% band centered at 633nm.

3.1 Manufacturing

The first set of four mirrors as designed above were diamond-turned from 2'' oxygen free high conductivity (OFHC) copper substrates in July 2011. The mirrors were inspected visually for artifacts; each has a conical central pit of with $\sim 10\mu\text{m}$ diameter and $5\mu\text{m}$ depth from the diamond turning tool. (Including this pit into the diffraction models shows them to have negligible effect on the system performance.) Residual rings from the diamond turning and shallow fissures of unclear origin are also present; all three of the effects can be seen in Fig. 8, which shows a microscope image of the center of the first set's M1. These visual artifacts can be removed by the application of a smoothing layer of PMMA followed by a layer of Al or silver to enhance reflectivity. A lithographic technique can also be employed to correct profile errors, as discussed in Balasubramanian *et al.* 2010.³

A Dektak profilometer was used to directly take measurements of the surface; a comparison of the designed mirror shape and the shape as measured with a profilometer. Unfortunately, this shows some significant disagreement between the designed and manufactured shape. The discrepancy is most severe near the outer

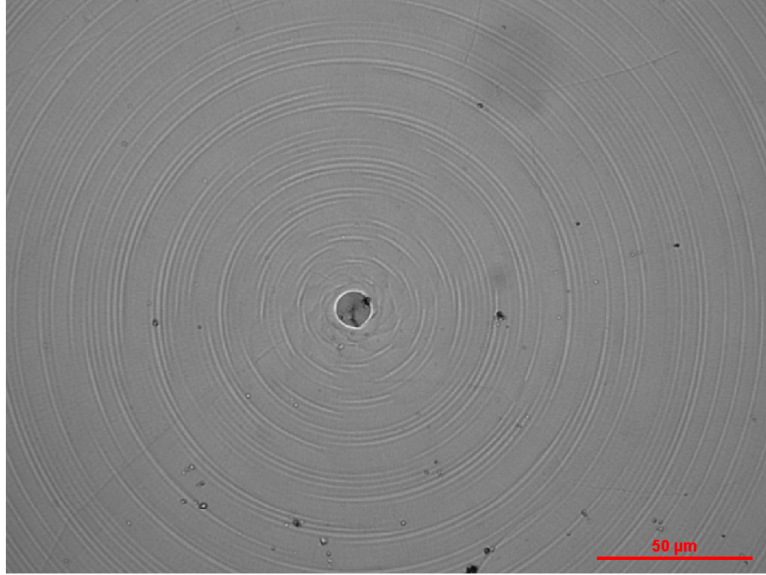


Figure 8. An image of the central pit on the first of the four mirrors; each one has a similar one in the center.

edges of the mirror, with the first of the four mirrors having over 2λ P-V shape error. These differences are shown in Fig. 9. At this level, these residual errors would destroy the performance of the four-mirror system, and hence we will be iterating on the manufacturing process to bring them to a level which could be managed effectively with deformable mirrors. Additionally, mirrors fabricated on SuperInvar substrates will provide thermal stability of the shapes thus improving system performance, and this is planned for subsequent iterations.

The same double-pass configuration described in Sec. 2 was used to test each of the two pairs individually. Fig. 10 and Fig. 11 show the residual wavefront for the first and second pairs, respectively. In both cases, piston, tip/tilt, and focus have been removed to allow the residuals to be examined. The first pair shows the full 30mm aperture, while the second uses only the inner 25mm; this was due to ringing near the edge of the aperture, which had a large enough amplitude to make it difficult to see the structure in the center. The residual is dominated by astigmatism and radially-symmetric structure from the manufacturing error; the astigmatism is primarily introduced by the tilt between the mirrors, and is well within the capability of a deformable mirror to remove, should it be required. (Zemax models of the mirrors, using Extended Aspheres to approximate the mirror surface with high-order polynomials, suggest that a few degrees of tilt between the mirrors will be an acceptable error for the system.)

4. SUMMARY

	Two-mirror system	Four-mirror system
Mirror cost (total)	\sim \$5K	\sim \$10K
Throughput	\sim 50%	$>$ 80%
Bandwidth	20%	20%
Apodizers	pre, post	pre
Broadband contrast	$\sim 1 \times 10^{-10}$ beyond $2\lambda/D$	$\sim 1.5 \times 10^{-9}$ beyond $1.5\lambda/D$
Measured contrast	5.5×10^{-7} , limited by system instabilities	TBD

Table 1. A comparison of as-built two- and four-mirror low-sag systems.

The manufacture and testing of low-sag mirrors is ongoing; we have presented some preliminary contrast

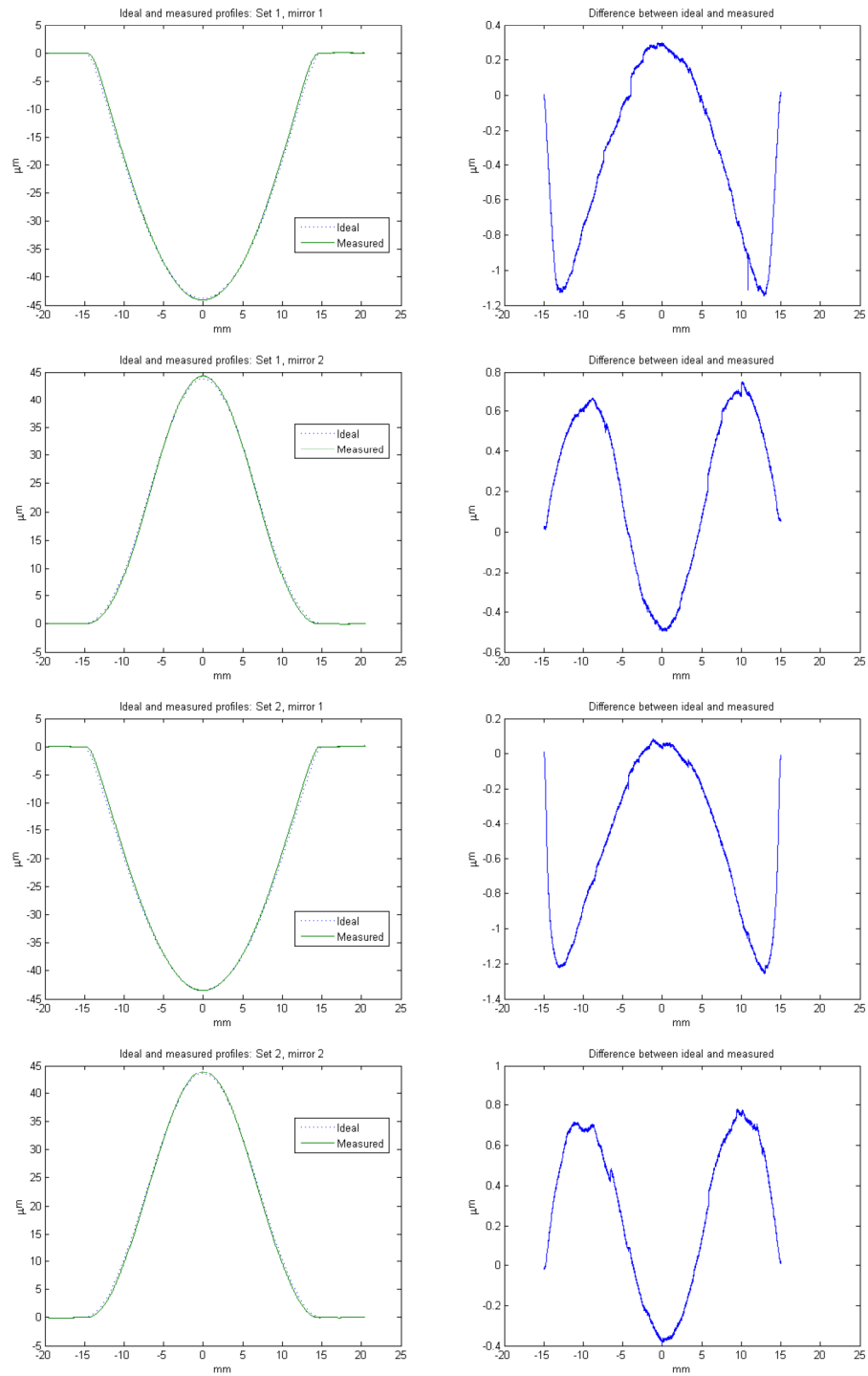


Figure 9. *Left column.* A comparison of the designed mirror shape and profilometer measurements of the mirrors as manufactured. *Right column.* The corresponding errors [designed - measured] between the ideal and measured shapes. All show residual $1\mu\text{m}$ -scale errors near the outer edge.

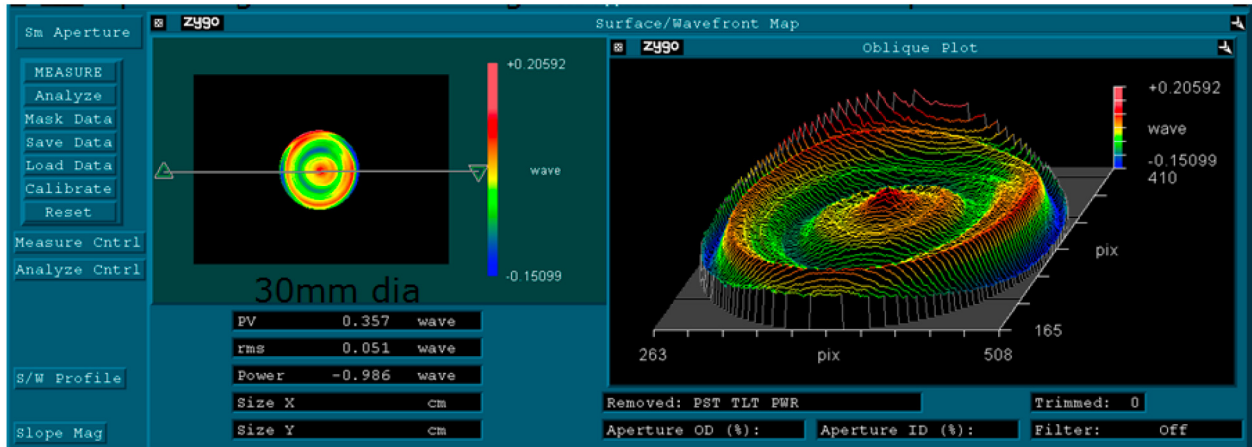


Figure 10. The residual wavefront error in the central 30mm of the first mirror pair. Piston, tip/tilt, and focus have been removed.

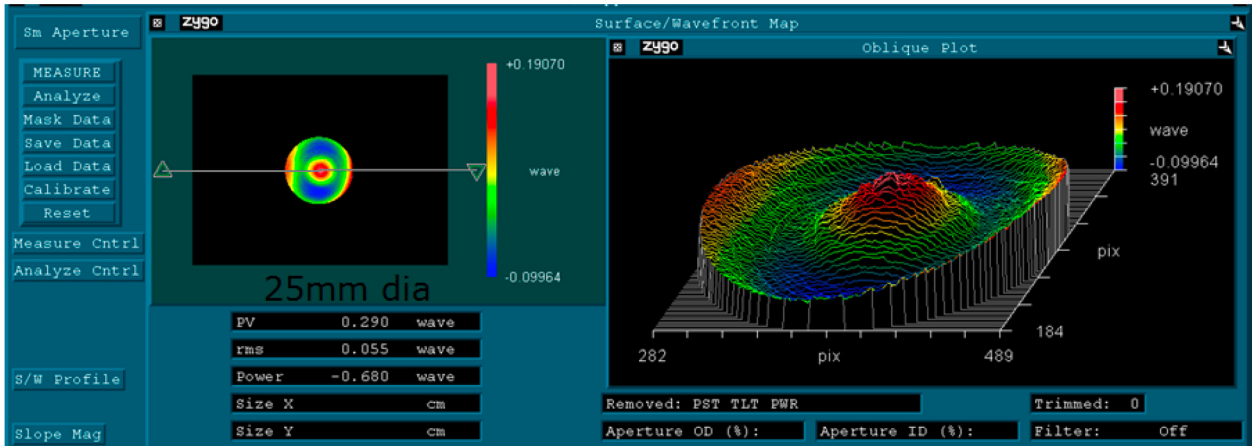


Figure 11. The residual wavefront error in the central 25mm of the second mirror pair. Piston, tip/tilt, and focus have been removed.

results for a single pair of mirrors and designs and initial manufacturing for a four-mirror set; this is the first time such a system has been proposed and analyzed. A comparison of two- and four-mirror designs is given in Table 1. Subsequently, we expect to iterate on the mirror manufacturing process to improve the residual errors on the manufacturing, and measure the double-pass wavefront for the full 4-mirror setup at JPL. We also plan to test a new iteration of mirrors on SuperInvar substrates in the Ames testbed with DMs and a pre-apodizer, in hopes of achieving better contrast for the system.

5. ACKNOWLEDGMENTS

This work was performed at the Jet Propulsion Laboratory, California Institute of Technology, under a contract with the National Aeronautics and Space Administration.

REFERENCES

- [1] Guyon, O., "Phase-induced amplitude apodization of telescope pupils for extrasolar terrestrial planet imaging," *Astronomy & Astrophysics* **404**, 379–387 (2003).
- [2] Traub, W. A. and Vanderbei, R. J., "Two-Mirror Apodization for High-Contrast Imaging," *The Astrophysical Journal* **599**, 695–701 (Dec. 2003).

- [3] Balasubramanian, K., Shaklan, S. B., Pueyo, L., Wilson, D. W., and Guyon, O., “Low-cost high-precision PIAA optics for high contrast imaging with exo-planet coronagraphs,” in [*Society of Photo-Optical Instrumentation Engineers (SPIE) Conference Series*], *Society of Photo-Optical Instrumentation Engineers (SPIE) Conference Series* **7731** (July 2010).
- [4] Meinel, A. B., Meinel, M. P., Stacy, J. E., Saito, T. T., and Patterson, S. R., “Wave-front correctors by diamond turning,” *Applied Optics* **25**, 824 (Mar. 1986).
- [5] Belikov, R., Pluzhnik, E., Witteborn, F. C., Lynch, D. H., Greene, T. P., Zell, P. T., and Guyon, O., “Laboratory demonstration of high-contrast imaging at inner working angles of $2\lambda/D$ and better,” in [*Society of Photo-Optical Instrumentation Engineers (SPIE) Conference Series*], *Society of Photo-Optical Instrumentation Engineers (SPIE) Conference Series* **8151** (2011).
- [6] Vanderbei, R. J. and Traub, W. A., “Pupil Mapping in Two Dimensions for High-Contrast Imaging,” *The Astrophysical Journal* **626**, 1079–1090 (June 2005).
- [7] Cady, E., “Design applications of propagation of amplitude functions in phase-induced amplitude apodization (piaa) systems,” (In preparation.).
- [8] Belikov, R., Kasdin, N. J., and Vanderbei, R. J., “Diffraction-based Sensitivity Analysis of Apodized Pupil-mapping Systems,” *The Astrophysical Journal* **652**, 833–844 (Nov. 2006).
- [9] Belikov, R., Give’on, A., Cady, E., Kay, J., Pueyo, L., and Kasdin, N. J., “Experimental Demonstration of Wavefront Estimation in a Shaped-Pupil Coronagraph,” in [*Bulletin of the American Astronomical Society*], *Bulletin of the American Astronomical Society* **38**, 1131 (Dec. 2006).
- [10] Pueyo, L., Shaklan, S., Give’On, A., and Krist, J., “Numerical propagator through PIAA optics,” in [*Society of Photo-Optical Instrumentation Engineers (SPIE) Conference Series*], *Presented at the Society of Photo-Optical Instrumentation Engineers (SPIE) Conference* **7440** (Aug. 2009).